Technical University of Denmark

DTU

Metamaterial localized resonance sensors: prospects and limitations

Jeppesen, Claus; Xiao, Sanshui ; Mortensen, N. Asger; Kristensen, Anders

DTU Library
Technical Information Center of Denmark

Metamaterial localized resonance sensors: prospects and limitations

C. Jeppesen,[1] **S. Xiao,**[2] **N. A. Mortensen,**[2] **and A. Kristensen**[1,*]

[1]*Department of Micro and Nanotechnology, Technical University of Denmark, DTU Nanotech, Building 345 East, DK-2800 Kongens Lyngby, Denmark*
[2]*Department of Photonics Engineering, Technical University of Denmark, DTU Fotonik, Building 345 West, DK-2800 Kongens Lyngby, Denmark*

[*]*anders@mailaps.org*

Abstract: The prospects and limitations of metamaterial localized resonance sensors are investigated theoretically and experimentally. Gold split-ring resonators are employed as the model system where the light induced *LC*-resonance yields a figure-of-merit, sensitivity divided by linewidth, up to 54 depending on the split-ring resonator design and engineering of the light-plasmon coupling. This highest measured value is comparable to quasi-static predictions, suggesting incremental improvements beyond this point. Further optimization attempts show the effect of inhomogeneous broadening giving some indication that the limits have been reached for this particular design and material choice.

© 2010 Optical Society of America

OCIS codes: (160.3918) Metamaterials,(220.4241) Nanostructure fabrication.

References and links

1. N. Fang, H. Lee, C. Sun, and X. Zhang, "Sub-diffraction-limited optical imaging with a silver superlens," Science **308**(5721), 534–537 (2005).
2. C. Jeppesen, R. B. Nielsen, A. Boltasseva, S. Xiao, N. A. Mortensen, and A. Kristensen, "Thin film Ag superlens towards lab-on-a-chip integration," Opt. Express **17**(25), 22543–22552 (2009).
3. I. I. Smolyaninov, Y.-J. Hung, and C. C. Davis, "Magnifying superlens in the visible frequency range," Science **315**(5819), 1699–1701 (2007).
4. J. Valentine, J. Li, T. Zentgraf, G. Bartal, and X. Zhang, "An optical cloak made of dielectrics," Nature Mater. **8**(7), 568–571 (2009).
5. B. Lahiri, A. Z. Khokhar, R. M. De La Rue, S. G. McMeekin, and N. P. Johnson, "Asymmetric split ring resonators for optical sensing of organic materials," Opt. Express **17**(2), 1107–1115 (2009).
6. T. Driscoll, G. O. Andreev, D. N. Basov, S. Palit, S. Y. Cho, N. M. Jokerst, and D. R. Smith, "Tuned permeability in terahertz split-ring resonators for devices and sensors," Appl. Phys. Lett. **91**(6), 062511 (2007).
7. E. Cubukcu, S. Zhang, Y.-S. Park, G. Bartal, and X. Zhang, "Split ring resonator sensors for infrared detection of single molecular monolayers," Appl. Phys. Lett. **95**(4), 043113 (2009).
8. A. W. Clark, A. Glidle, D. R. S. Cumming, and J. M. Cooper, "Plasmonic split-ring resonators as dichroic nanophotonic DNA biosensors," J. Am. Chem. Soc. **131**(48), 7615–17619 (2009).
9. N. A. Mortensen, S. Xiao, and J. Pedersen, "Liquid-infiltrated photonic crystals: enhanced light-matter interactions for lab-on-a-chip applications," Microfluid. Nanofluid. **4**(1-2), 117–127 (2008).
10. D. Dorfner, T. Zabel, T. Hurlimann, N. Hauke, L. Frandsen, U. Rant, G. Abstreiter, and J. Finley, "Photonic crystal nanostructures for optical biosensing applications," Biosens. Bioelectron. **24**(12), 3688–3692 (2009).
11. C. Jeppesen, N. A. Mortensen, and A. Kristensen, "Capacitance tuning of nanoscale split-ring resonators," Appl. Phys. Lett. **95**, 193108 (2009).
12. J. Zhang, S. Xiao, C. Jeppesen, A. Kristensen, and N. A. Mortensen, "Electromagnetically induced transparency in metamaterials at near-infrared frequency," Opt. Express **18**(16), 17187–17192 (2010).
13. Y. Sivan, S. Xiao, U. K. Chettiar, A. V. Kildishev, and V. M. Shalaev, "Frequency-domain simulations of a negative-index material with embedded gain," Opt. Express **17**(26), 24060–24074 (2009).

14. V. A. Fedotov, A. Tsiatmas, J. H. Shi, R. Buckingham, P. de Groot, Y. Chen, S. Wang, and N. I. Zheludev, "Temperature control of Fano resonances and transmission in superconducting metamaterials," Opt. Express **18**(9), 9015–9019 (2010).
15. L. J. Sherry, R. Jin, C. A. Mirkin, G. C. Schatz, and R. P. Van Duyne, "Localized surface plasmon resonance spectroscopy of single silver triangular nanoprisms," Nano Lett. **6**(9), 2060–2065 (2006).
16. F. Wang and Y. R. Shen, "General properties of local plasmons in metal nanostructures," Phys. Rev. Lett. **97**(20), 206806 (2006).
17. M. Svedendahl, S. Chen, A. Dmitriev, and M. Kall, "Refractometric sensing using propagating versus localized surface plasmons: a direct comparison," Nano Lett. **9**(12), 4428–4433 (2009).
18. P. B. Johnson and R. W. Christy, "Optical constants of noble metals," Phys. Rev. B **6**(12), 4370–4379 (1972).
19. M. A. Ordal, L. L. Long, R. J. Bell, S. E. Bell, R. R. Bell, R. W. Alexander, and C. A. Ward, "Optical properties of the metals Al, Co, Cu, Au, Fe, Pb, Ni, Pd, Pt, Ag, Ti, and W in the infrared and far infrared," Appl. Opt. **22**(7), 1099–1119 (1983).
20. M. Stockman, S. Faleev, and D. Bergman, "Localization versus delocalization of surface plasmons in nanosystems: can one state have both characteristics?" Phys. Rev. Lett. **87**(16), 167401 (2001).
21. S. Zhang, D. A. Genov, Y. Wang, M. Liu, and X. Zhang, "Plasmon-induced transparency in metamaterials," Phys. Rev. Lett. **101**(4), 047401 (2008).
22. H. Liu, D. A. Genov, D. M. Wu, Y. M. Liu, Z. W. Liu, C. Sun, S. N. Zhu and X. Zhang, "Magnetic plasmon hybridization and optical activity at optical frequencies in metallic nanostructures," Phys. Rev. B **76**(7), 073101 (2007).
23. J. Henzie, M. H. Lee, and T. W. Odom, "Multiscale patterning of plasmonic metamaterials," Nat. Nanotechnol. **2**(9), 549–554 (2007).
24. X. Yu, L. Shi, D. Han, J. Zi, and P. V. Braun, "High quality factor metallodielectric hybrid plasmonic-photonic crystals," Adv. Funct. Mater. **20**(12), 1910–1916 (2010).
25. A. V. Kabashin, P. Evans, S. Pastkovsky, W. Hendren, G. A. Wurtz, R. Atkinson, R. Pollard, V. A. Podolskiy, and A. V. Zayats, "Plasmonic nanorod metamaterials for biosensing," Nature Mater. **8**(11), 867–871 (2009).
26. X. Fan, I. M. White, S. I. Shopoua, H. Zhu, J. D. Suter, and Y. Sun, "Sensitive optical biosensors for unlabeled targets: a review," Anal. Chim. Acta **620**(1-2), 8–26 (2008).

1. Introduction

Metamaterials are artificially structured materials that obtain their properties from their mesoscopic unit cell structure rather than from the constituent materials. The focus of metamaterials has primarily been on their unique optical properties such as a negative refractive index, that enables the fabrication of exotic devices e.g. near-field superlenses [1, 2], hyperlenses [3], and invisibility cloaks [4]. However, lately there has also been considerable interest in using metamaterials as refractive index sensors. Metamaterials consisting of split-ring resonators (SRRs) are among the potential sensor candidates. SRRs have already been employed to detect thin polymer layers [5], Si nanospheres in solution [6], organic monolayers [7] and DNA [8]. SRR sensors have a competitive sensitivity to e.g. photonic crystal based sensors [9, 10] but with the wide resonance peak, see e.g. [11], being a major drawback. Several suggestions have been made to improve this including utilization of EIT-like concepts [12], embedding the SRRs in optical gain materials [13], and fabricating SRRs out of superconducting materials [14].

In this paper, we investigate the limits of metamaterial based sensors and derive an analytical expression for the figure-of-merit [15]

$$\text{FOM} = \frac{|\Delta\lambda/\Delta n|}{\delta\lambda} = \frac{Q}{\lambda}\left|\frac{\Delta\lambda}{\Delta n}\right|, \tag{1}$$

which favors a large sensitivity $\Delta\lambda/\Delta n$ and a narrow resonance linewidth $\delta\lambda = \lambda/Q$, which is central for the quantification of minute refractive-index changes. The quality factor Q has contributions from coupling, radiation loss, and inhomogeneous broadening, i.e. $Q = 1/(Q_0^{-1} + Q_{\text{coup}}^{-1} + Q_{\text{rad}}^{-1} + Q_{\text{inhom}}^{-1})$. In addition, there is an intrinsic Q_0 related to the ohmic damping of the plasmons. Surprisingly, in the quasi-static limit Q_0 has a universal nature [16]. The FOM inherits this universality, carrying no information on the detailed geometry of the plasmonic resonator. For common plasmonic metals (such as Au, Ag, and Al) this allows us to estimate
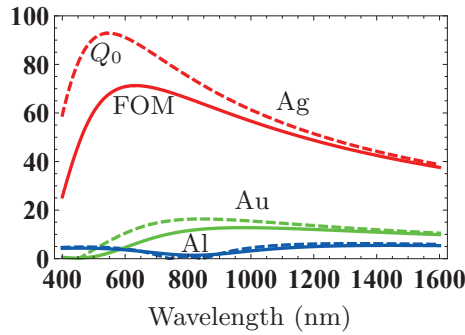
Fig. 1. The figure-of-merit (solid lines) in the quasi-static limit for three common plasmonic metals (Au, Ag, and Al). The dashed lines show corresponding results for the quality-factor.

typical FOMs in the range from 5 to 80, depending on the particular resonance frequency and the material of choice. The derived expression is tested by a SRR based model system where the coupling of bright and dark plasmonic elements is exploited to narrow the linewidth of the fundamental LC-resonance for all-gold SRRs.

2. Theory

Wang and Shen [16] used quasi-static arguments (assuming that $k\Lambda \ll 1$, with Λ being a characteristic length scale of the unit cell) to show that for metal structures surrounded by air, plasmonic localized resonances would have a universal quality factor

$$Q_0 = \frac{\omega \frac{\partial \varepsilon'_m}{\partial \omega}}{2\varepsilon''_m}, \quad k\Lambda \ll 1, \tag{2}$$

where $\varepsilon_m = \varepsilon'_m + i\varepsilon''_m$ is the complex permittivity of the metal. This result implies that any efforts of improving the sharpness of the plasmon resonance will be unfruitful, since the Q is only determined by the choice of metal and resonance frequency. Following the same lines we may derive a universal value of the FOM in the quasi-static limit. In particular, it can be shown that the sensitivity becomes $\partial \lambda / \partial n = (-\varepsilon'_m/\varepsilon''_m)\lambda/Q_0$ so that Eq. (1) becomes

$$\text{FOM} = \frac{|\varepsilon'_m|}{\varepsilon''_m}, \quad k\Lambda \ll 1. \tag{3}$$

A similar result was reported recently by Svedendahl *et al.* [17]. Interestingly, this intrinsic FOM is highly dependent on the plasmon damping while at the same time fully independent of the underlying geometrical details of the resonant plasmonic structure. Improving the geometrical properties will thus mainly serve to minimize radiation and coupling degradation of the intrinsic FOM. For larger resonator structures, the quasi-static assumption is not fulfilled, but as emphasized in Ref. [16], the predictions may still serve as important guidelines. Fig. 1 illustrates Eq. (2) and Eq. (3) for three often used metals in metamaterials with data taken from [18, 19]. As seen, there is a vast difference in FOM between the chosen metals with silver being the best and aluminum being the worst. Most importantly, we emphasize the characteristic scale of the FOM, indicating that for localized plasmonic resonances in typical metal nanostructures the FOM is unlikely to exceed the range 10 to 10^2. For the majority of experimental studies, gold is the preferred material for nanostructures because it is relatively stable over time whereas silver rapidly oxidizes in an atmospheric environment.

3. Design and fabrication

To narrow the linewidth of the fundamental *LC*-resonance, we employ the coupling of bright and dark plasmonic elements. Bright and dark elements were first introduced by Stockman *et al.* [20]. The bright elements are easily excited by free-space radiation and the radiation dissipation limits their quality factor. When excited, the bright element can excite neighboring dark elements via near-field coupling. The absent direct radiation coupling results in a high quality factor for the dark elements, thus mainly being limited by the loss of the metal [21]. For a SRR, a bright element requires the arms to be aligned perpendicular to the radiation polarization whereas rotating the SRR by $\pm\pi/2$ leads to a dark element. For SRR based devices some optical activity occurs [22] but most of the energy stored in the dark element is re-radiated through the bright element. Here, the effect of the bright and dark elements is investigated by defining a unit cell of 2×2 SRRs and then changing the number of bright elements from four to one.

In fabrication, a 180 nm thick layer of EBL resist, ZEP520A (Zeon Corp., Tokyo, Japan) is spincoated onto a 1 mm thick fused silica substrate. A 15 nm aluminium layer is thermally deposited on top of the ZEP layer to prevent charge accumulation during EBL. A 1.2×1.2 mm^2 area is written with a 100 kV JEOL JBX-9300FS EBL tool (200 μC/cm^2 dose, 2 nA current, 6 nm spotsize). The aluminium layer is then removed in MF-322 (Rohm and Haas, Coventry, UK) and the positive ZEP resist is developed in ZED-N50 (Zeon Corp.) developer. A brief O$_2$ plasma descum process is applied to remove residual resist before 50 nm Au is deposited by electron beam deposition. The final lift-off is performed by using Remover 1165 (Rohm and Haas). The fabricated samples are given in Fig. 2.
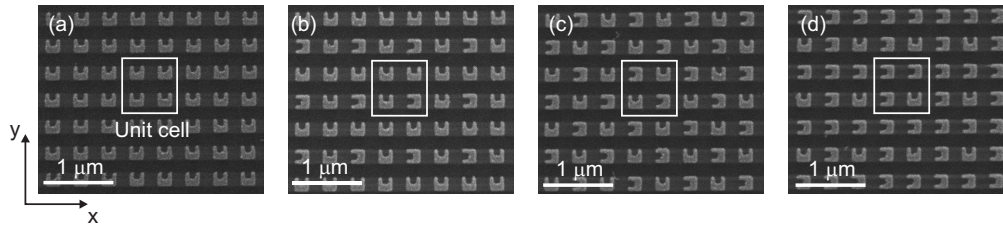

Fig. 2. SEM micrograph of the four unit cell configurations. The incident light is polarized along the *x*-direction. The samples have a sidelength ℓ=200 nm, height h=90 and a period Λ=400 nm. (a) 4 bright SRRs per unit cell. (b) 3 bright + 1 dark SRRs per unit cell. (c) 2 bright + 2 dark SRRs per unit cell. (d) 1 bright + 3 dark SRRs per unit cell.

4. Optical characterization

The transmission spectra are recorded in a free space setup using a supercontinuum light source (500-1750 nm, SuperK SCB-Compact 100-PC) and an optical spectrum analyzer (400-1750 nm, Ando AQ-6315E). The output beam is collimated and broadened to a 200 μm spot via a parabolic mirror. Then the light is linearly polarized by a Glan-Thompson polarizer before it reaches the sample. After traversing the sample, the beam is focused by another parabolic mirror and collected with an output fiber with a 10 μm core diameter leading to the spectrum analyzer. The transmission measurements are summarized in Fig. 3.

By combining bright and dark elements, the linewidth is reduced from 220 nm in Fig. 3(a) to 29 nm in Fig. 3(d), which is a 87% reduction. At the same time the resonance depth exhibits a 40% (0.88 to 0.53) signal decrease. The fact that the relative narrowing is larger than the relative signal modulation, demonstrates the superiority of the latter design. Hence, the energy
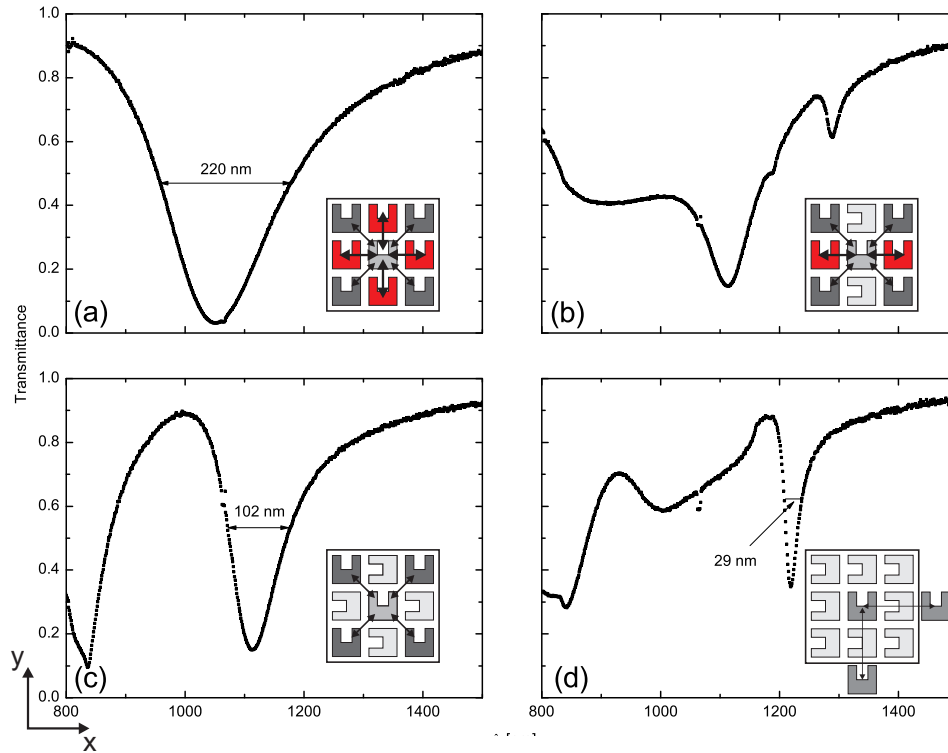
Fig. 3. Transmission measurements of the four unit cell configurations. The incident light is polarized along the *x*-direction. The insets show the nearest-neighbor interactions of the bright elements with the arrow width denoting the SRR-SRR coupling strength. (a) 4 bright SRRs per unit cell. (b) 3 bright + 1 dark SRRs per unit cell. (c) 2 bright + 2 dark SRRs per unit cell. (d) 1 bright + 3 dark SRRs per unit cell. The small signal disturbance at 1064 nm is an artifact from the pumping laser of the supercontinuum light source.

dissipation from SRR-SRR coupling is significantly less than the energy dissipation steming from the coupling to the radiation field.

The insets in Fig. 3 illustrate the nearest-neighbor coupling of the bright element. Due to the coupling, the measured signal from one SRR within the array, $A_{\mathrm{SRR_{meas}}}$, is a sum of several contributions

$$A_{\mathrm{SRR_{meas}}} = \sum A_{\mathrm{SRR}} + c_1 \times A_{\mathrm{nn}} + c_2 \times A_{\mathrm{nnn}} \cdots, \qquad (4)$$

where c_1 and c_2 are configuration dependent positive integers and the subscripts nn and nnn denote nearest-neighbor and next-nearest-neighbor, respectively. The strongest contribution comes from the SRR itself (A_{SRR}) and for Fig. 3(a), (c), and (d) the nearest-neighbor term dominates. However, for Fig. 3(b) there are only 2 nearest-neighbors and 4 next-nearest-neighbors so that the dominance is less pronounced, resulting in a double dip. Even contributions from SRRs further away can be seen, which illustrates the vast dominance of the nearest-neighbor terms in Fig. 3(a), (c), and (d) where no other contributions to the fundamental *LC*-resonance are clearly observable. Note that the resonance at Λ=850 nm in Fig. 3(c) and (d) is a higher order mode and therefore not considered here. The overall narrowing can be seen as a step towards the intrinsic response of a single isolated SRR.

Fig. 3(d) illustrates the potential of SRR based sensors. The transmission spectrum for a

slightly more optimized structure in terms of the individual SRR geometry as well as the period Λ is given in Fig. 4. The sensitivity was measured by fluidic tuning of the cladding material. A
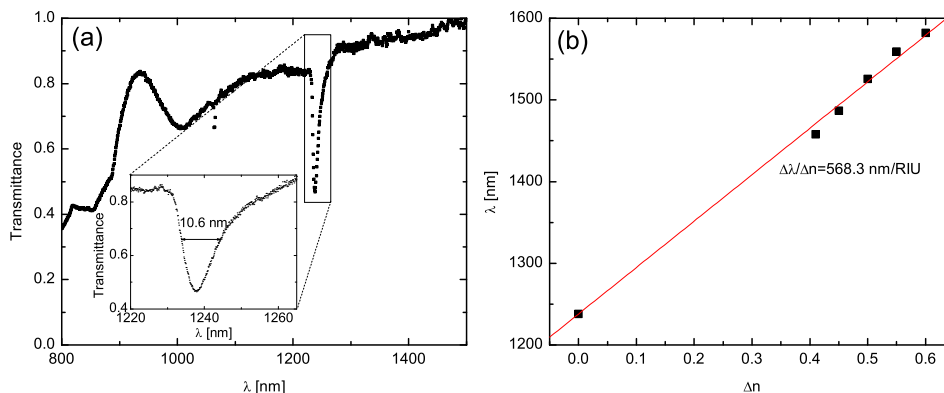

Fig. 4. Transmission measurements of optimized "1 bright + 3 dark" structure. The SRRs have ℓ=200 nm, h=90 nm, Λ=425 nm. (a) Standard transmission measurement with air as cladding (b) Sensitivity curve based on transmission measurements for a dynamic range of 0.6 RIU.

sensitivity of 568.3 nm/RIU$\pm$6.9 nm/RIU and a linewidth of 10.6 nm, translates into a FOM of 54. This is one of the largest FOM's reported at visible or infrared frequencies [23,24]. Whereas the sensitivity is typical for this type of structure, the linewidth is extraordinary compared to typical values for similar designs [11].

Numerical simulations (CST Microwave Studio) have indicated that by increasing the height h the resonance could be additionally narrowed without affecting the sensitivity. However, h=100 nm did not further improve the linewidth. To the contrary the linewidth was widening to $\sim$12-13 nm. The increase is attributed to a poorer lift-off process, hence larger inhomogeneous broadening. This indicates that the limits of optimization has been reached for this particular SRR design and material choice.

5. Discussion and conclusion

Equation (3) shows that the fundamental limitation of localized plasmon based sensors scales with the material loss. Metals are commonly used in metamaterials at the expense of a high loss compared to semiconductors or dielectrics. Despite recent advances for guided plasmon modes in nanorod arrays [25], metallic metamaterials are unable to obtain the same figure-of-merits as seen in LSPR or interferometry based devices [26]. Hence, with present knowledge, metamaterial-based resonant structures do not appear as obvious candidates for a competitive refractometric sensing platform.

In conclusion, we have demonstrated the limitations of metamaterial localized resonance sensors theoretically and experimentally. Gold split-ring resonators have been employed as the model system yielding a figure-of-merit of up to 54 depending on the split-ring resonator design and the light-plasmon coupling. The measured values are comparable to quasi-static predictions, suggesting incremental improvements beyond this point.